STRUCTURAL TESTING OF ENHANCED

POST-TENSIONED CONCRETE MASONRY WALLS

by Peter T. Laursen and Jason M. Ingham

ABSTRACT

The in-plane response of post-tensioned concrete masonry walls with unbonded tendons, incorporating strengthened masonry and enhanced energy dissipation, is examined by means of structural testing. An introduction to the testing programme is followed by a presentation of the results from structural testing of five fully grouted walls. Discussion of the results is concerned with wall structural response in terms of flexural strength, displacement capacity, tendon stress and masonry vertical strain, and makes comparison with testing of unconfined (ordinary) post-tensioned concrete masonry walls.

Keywords: concrete masonry, confinement, structural wall, prestressing, post-tensioning, structural testing, in-plane response, rocking, seismic design.

Peter T. Laursen received his Ph.D. in Structural Engineering at the University of Auckland, New Zealand, 2002. Dr. Laursen is currently a Bridge Engineer with COWI A/S, Denmark, and principally works in the field of cable stayed and suspension bridges. In 2000 he received the ASTM International Committee C15 Alan W. Yorkdale Memorial Award.

ACI member Jason M. Ingham is a Senior Lecturer in the Department of Civil and Environmental Engineering at the University of Auckland. He received his Ph.D in Structural Engineering from the University of California at San Diego, and his research interests include the study of reinforced and prestressed concrete and masonry structures.

RESEARCH SIGNIFICANCE

This paper presents the results from in-plane cyclic structural testing of five unbonded post-tensioned concrete masonry (PCM) walls. These wall tests were an integral part of a doctoral study conducted at the University of Auckland, New Zealand, investigating the seismic analysis and design of PCM walls (Laursen, 2002). The study aligned with recent research into unbonded post-tensioned concrete walls, e.g. Nakaki et al. (1999), Kurama et al. (2002) and Holden et al. (2003).

INTRODUCTION

Previous testing reported by Laursen and Ingham (2001) explored single-storey post-tensioned concrete masonry walls constructed of unconfined (ordinary) concrete masonry. It was found that such walls typically had reliable displacement (drift) capacity of up to 1%. However, the limited strain capacity of unconfined masonry resulted in masonry crushing and subsequent strength degradation, prohibiting development of further reliable drift capacity.

The principal objective of the testing series reported here was to extend and augment previous research considering unconfined masonry by investigating several different means of masonry strengthening that were expected to result in superior reliable drift capacity, say of the order of 1.5%-2%. According to Laursen et al. (2002), drift demands of such magnitude are likely to be encountered in structural systems utilising unbonded post-tensioned walls when subjected to severe seismic loading because of the inherent limited structural damping.

A second objective of this testing series was to investigate the use of supplementary structural damping, which may be required to control wall displacement demand during strong ground motion as a consequence of the limited hysteretic energy dissipation of PCM. As a potentially simple solution, ‘dog-bone’-type dampers were incorporated in one wall test to explore the suitability of this type of devise.

CONSTRUCTION DETAILS

Wall specifications

Wall dimensions are specified in Table 1, with each wall having an associated designation describing its geometry and construction. All test units were constructed to the same dimensions, being a length, l_w, of 3.0 m, a height, h_w, of 2.6 m and a thickness, b_w, of 0.14 m using 15 series (140 mm nominal thickness) concrete masonry units. The wall designations follow the convention: FG indicates fully grouted, L3.0 indicates that the wall was 3.0 m long, W15 indicates a nominal wall thickness of 150 mm and P2 means that two prestressing bars were imbedded in the wall. CP, HB, ED and CA represent confining plates, high strength blocks, energy dissipation and constant axial load, respectively.

The main part of each wall was constructed with full height concrete masonry units (nominally 200 mm high). For walls 2, 3 and 4, the lower corner in compression during push loading was constructed with half-height concrete masonry units (100 mm nominal height), as indicated in Fig. 1, with an extent of 600 mm vertically and 1200 mm horizontally. The asymmetrical use of half height units in the bottom corners enabled a direct comparison between the effectiveness of different confining plate details. The half height units were obtained from the masonry block supplier, though some webs needed to be modified to accommodate the shear reinforcement. Both lower corner units of Wall 5 were fabricated specially for this test using high strength steel fibre reinforced concrete (not shown in Fig. 1). The self-weight of all walls, including the loading beam, was N = 41 kN.

Confining plates embedded in the toe regions (flexural compression zones) are indicated on Fig. 1. These plates were placed in all bed joints in the lowest 600 mm above the foundation, embedded with mortar on both sides for best integrity. In the following, the designations U200, CP200 and CP100 refer to ‘unconfined full height grouted concrete masonry’ (main body of all walls), ‘confined full height grouted concrete masonry’ (confined region bottom

left corner in Fig. 1) and 'confined half height grouted concrete masonry' (confined region bottom right corner in Fig. 1), respectively. Further information on enhancement of the masonry performance caused by confining plates may be found in Priestley and Elder (1983).

Two high strength corner units were manufactured to the exact dimension of ordinary 15 Series concrete masonry units (390 mm long, 190 mm high and 140 mm deep). These units were located in each lower corner (position indicated in Fig. 6(e)) to provide durable pivoting points for wall rocking, thus isolating the above masonry units from extreme strain.

Walls 3 and 4 had 2 x HD10 (10 mm deformed bar, 430 MPa nominal yield strength) embedded horizontally at 400 mm vertical intervals. No shear reinforcing was provided in the other walls (except for 2 x HD10 placed in top course to provide a bond beam).

Energy dissipaters were embedded centrally in Wall 4 as shown in Fig. 1. These were of the so-called 'dog bone'-type, and were expected to provide hysteretic damping as a result of yielding in tension and compression. The milled part of the bars were designed such that the axial prestressing force (kept constant throughout testing) comfortably could yield the bars in compression, thus forcing the wall back to its original alignment upon unloading. An energy dissipater yield force to prestressing force ratio of approximately 1:3 was chosen for this test, reflected by nominal yield strength of the reduced diameter section of each energy dissipation bar of approximately 100 kN and axial force in the wall due to the prestressing of 617 kN. Fig. 2 illustrates the dimensions of the energy dissipation bars. The bars were made of 20 mm reinforcing steel with nominal yield strength of 500 MPa. The bar diameter was reduced to 16 mm over a length of 375 mm to ensure that the bar yielded in a well defined region adjacent to the wall base and to limit strain such that an extreme wall displacement excursion would not cause bar rupture. The bar was confined by heavy steel tube with an inside diameter of 27 mm and a length of 555 mm to ensure that the section of bar intended to yield

would not buckle when put into compression. The tube was filled with dental plaster and the dissipation bars remained unbonded over a length of 465 mm, as shown in Fig. 2.

All walls were prestressed with two 23 mm VSL thread bars placed concentrically at ±400 mm from the wall centreline, located to accommodate the masonry modular dimensions, be symmetric, and provide an approximately uniform distribution of prestress to the top plane of the wall while minimising the magnitude of tendon strain developed during wall rocking. The prestressing tendons were unbonded over their entire length in order to maximise the magnitude of lateral deformation associated with the onset of tendon yield, with a typical unbonded length of 3.5 m, including unbonded lengths in the foundation (300 mm), loading beam (400 mm) and load cells on top of the loading beam (200 mm). An additional tendon length of 300 mm due to hydraulic jacks in the vertical loading system applied in the case of Walls 3 and 4. The wall initial prestressing force and axial force ratios (due to prestressing and self-weight) replicated values expected in practice and are given in Table 1, with the total axial force expressed as a ratio of the force necessary to cause axial crushing of the masonry. Unfortunately, the left prestressing bar (bar closest to strong wall) of Wall 1 tore out of the foundation anchorage during the initial stressing, thus the designation 'P1'. Constant axial load in the prestressing bars was applied for Walls 3 and 4, such that the prestressing bars did not yield as the wall was displaced laterally.

Wall construction

Prior to wall construction, the prestressing bars were inserted into the foundation and encased by ducting to ensure proper isolation from the grout. The walls were constructed in running bond by experienced blocklayers under supervision, using standard grey precast concrete masonry units and commercial trade mortar, being a bagged 1:4 cement:sand blend containing water improver. Open-ended concrete masonry units were used to avoid having to thread the masonry units onto the 4 m long prestressing bars. Grouting with ready-mixed regular block

fill having a specified characteristic strength of 17.5 MPa, and containing a commercially available expansion agent, was generally performed the following day. Vibration of the grout was carried out for Walls 3 and 4, with all walls fully grouted to ensure enhanced performance when compared with their partially grouted equivalent. As recorded in Table 1, there was distinct variation in the quality of grout delivered, with Walls 2 and 5 having strengths markedly lower than the others.

Material properties

Average masonry material properties were determined by material testing, typically in samples of three. The masonry crushing strength f'_m and age of the wall at the day of testing are given in Table 1.

High strength masonry units were fabricated in the laboratory using steel fibre reinforced concrete, having an average 50 mm cube crushing strength of 131 MPa and a standard deviation of 2 MPa. Whilst high strength masonry units are not currently commercially available in New Zealand due to a lack of demand, there is little impediment to their manufacture.

VSL 23 mm diameter high strength threaded bars were used in all wall tests and had the typical properties: yield strength of 970 MPa, ultimate strength of 1160 MPa, ultimate strain of 8% and modulus of elasticity of 190 GPa, all of which were confirmed by material testing.

TESTING DETAILS

Test setup

Wall testing reported in this paper was conducted using the setup shown in Fig. 3, consisting of a reusable foundation and loading beam. Notably, no effort was made to replicate axial gravity and live loads from suspended floors, as these loads were considered to be generally

comparable to a component of the applied post-tensioning force given the rigidity of the loading beam and the associated transfer of force to the upper plane of the wall.

Fig. 4 schematically shows typical wall instrumentation. Lateral load was measured by two load cells, LCH1 and LCH2, positioned in series with the lateral hydraulic actuators, and lateral displacement at the top of the wall (height of 2.8 m above base) was measured by the displacement transducers DISP1 and DISP2. Wall flexural deformation and vertical strain were measured by instruments denoted 'F'. Relative sliding displacements between loading beam/wall, wall/foundation and foundation/strong floor were measured by instruments denoted 'S'. 'DIGI' denotes digital display displacement transducers that were employed to confirm lateral displacement measurements. Axial force in the prestressing bars was measured by the load cells LCPR1 and LCPR2. Flexural instrumentation F1-F4, F9-F12 and F17-F28, shown in Fig. 4, were mirrored on the wall back side.

Dowel bars were embedded in the foundation for Walls 3 and 4, as indicated in Fig. 1. The dowels were made from HD20 reinforcing steel (430 MPa nominal yield strength), had an embedment length into the foundation of 200 mm and protruded 80 mm into the wall. The deformations were removed from the 80 mm length and the bar was greased and encased in a sleeve to ensure that no bond was formed between the dowel and surrounding grout.

Sliding blocking devices were mounted on the foundation beam by each end of the wall. These devices were intended to block wall sliding, should this occur. The height of the devices varied from 70 mm for Walls 1, 2, 3 and 5, to 150 mm for Wall 4. Gaps of 3 mm (nominal) were present between the wall ends and the sliding blocking devices in the unloaded state.

Testing procedure

Cyclic structural testing was conducted according to the procedure outlined by Park (1989), with the ductility one displacement here termed 'displacement level one' or D1. After definition of D1, the walls were cycled to D2, D4, D6, etc. until failure, with Dn being defined as n times D1. Prior to executing this loading procedure, serviceability limit state level force cycles were applied to some walls in order to investigate the un-cracked stiffness and the initial crack formation.

Predicted nominal flexural strength

For a symmetric distribution of post-tensioning and gravity actions, the nominal flexural strength, M_n, is defined by the New Zealand masonry design standard NZS 4230:1990:

$$M_n = V_f h_e = (P + \Delta P)\left(\frac{l_w}{2} + e_t - \frac{a}{2}\right) + N\left(\frac{l_w}{2} - \frac{a}{2}\right) \quad (1)$$

$$a = \frac{P + \Delta P + N}{\alpha f'_m b_w} \quad (2)$$

$$e_t = \frac{l_w \Delta P}{6(P + \Delta P)} \quad (3)$$

V_f is the base shear corresponding to M_n, P represents the initial prestress force (no lateral load applied to wall), ΔP is the total tendon force increase due to wall deformation at V_f and N is the axial load at the base of the wall due to live and dead load. The equivalent rectangular compression zone length, a, is a function of the axial forces on the section, the masonry compressive strength, f'_m, the wall width b_w and α = 0.96 for confined grouted concrete masonry. Eqn. (3) defines the effective tendon force eccentricity, e_t, with respect to the initial prestressing force and the tendon force increase based on the assumption of uniformly distributed prestressing steel. In the absence of suitable procedures for estimating ΔP at the

time of testing, the tendon force increase at nominal strength was estimated to be 50 kN for Walls 2 and 5 and zero for Wall 1. Walls 3 and 4 had constant axial load applied to the prestressing bars, i.e. $\Delta P = 0$. Flexural strength increase of Wall 4, due to the yielding energy dissipators, was not taken into account when estimating V_f.

Predicted masonry shear strength

The predicted masonry shear strength, v_m (stress), was calculated according to Eqn. (4) as advocated by Paulay and Priestley (1992):

$$v_m = 0.136\sqrt{f'_m} + 0.24\frac{P+N}{A_g} \leq 1.04 \text{ MPa} \quad (4)$$

where $A_g = l_w b_w$. Shear strength due to shear reinforcing was calculated using the equation:

$$V_{st} = A_v f_{vy} \frac{d}{s} \quad (5)$$

where A_v is the steel area with centre to centre spacing s, $d = 0.8\ l_w$ and f_{vy} is the nominal yield strength of the shear reinforcing. The predicted wall shear strengths $V_s = v_m \cdot A_g + V_{st}$ are listed in Table 2. The initial prestress force P was used in this calculation.

TEST RESULTS

This section describes the behaviour of the five walls and presents the measured masonry compression toe strains at various wall states. General wall behaviour is summarised in Table 2, where V_{max} is the maximum lateral force recorded and d_{vmax} is the corresponding displacement. The ultimate displacement capacity, d_u, is defined as the point at which the lateral wall strength had degraded below 80% of V_{max}. The ultimate drift capacity is defined as $\gamma_u = d_u/h_e$ with $h_e = 2.8$ m.

Rocking response was recorded for all wall tests, with a single large crack opening up along the wall-foundation construction joint and no distributed flexural cracks observed. A single inclined crack was observed for Wall 2 as a result of loading in the pull direction, and a similar crack was observed for Wall 5. Both of these walls contained no shear reinforcing. Cracking occurred in the centre of Wall 4, presumably due to bond stress associated with transfer to the masonry of the tensile force generated within the energy dissipation bars during wall rocking. At nominal flexural strength, $V_f = M_n/h_w$, wall softening occurred due to the initiation of rocking. Tendon yielding was experienced in Walls 1, 2 and 5, which all had tendons permanently anchored in the foundation and loading beam. The tendons in Walls 3 and 4 remained elastic during testing.

The failure mode was characterised by localised masonry crushing in the compression toe regions, resulting in gradual strength degradation. Using CP200 masonry, inelastic masonry strain was found to be concentrated in the lowest course (200 mm), whereas when using CP100 masonry inelastic vertical strain penetrated into the second and third course above the foundation (200-300 mm). Failure of the compression toes for Wall 5 was initiated by crushing of the ordinary masonry course (U200) just above the high strength units.

Considerable sliding displacement between wall and foundation was recorded for Walls 1-3.

Hysteretic energy dissipation was increased considerably for Wall 4 because of the embedded 'dog-bone' energy dissipation bars, in comparison with the other walls.

Force-displacement response

Fig. 5, depicting the force-displacement response for all fully grouted walls, demonstrates the nearly non-linear elastic behaviour exhibited by the tested unbonded post-tensioned walls prior to toe crushing, with the exception of Wall 4. It is seen that the walls returned to their original alignment, even after large displacement excursions. This type of response may be

categorised as ‘origin oriented’. For all walls, except Wall 4, the individual curves for each excursion appear pinched, implying little hysteretic energy dissipation. It is noted that the term ‘elastic’ in a rigorous sense indicates reversibility and no accumulation of damage. In reality the walls did accumulate damage from the onset of tendon yielding and masonry crushing, causing a reduction in wall stiffness. Thus the behaviour was termed ‘nearly’ non-linear elastic.

None of the walls exhibited symmetrical response in the push and pull directions. Wall 1 was tested in the pull direction only. Wall 2 was tested cyclically (alternating push and pull excursions) for displacements up to D2 (5 mm) but monotonically thereafter, first in the push direction and then in the pull direction, because of an inclined crack (Fig. 6(b)) that occurred while pulling to -D2 (-5 mm) which caused concern about wall integrity in the pull direction. Continued testing in the push direction was adopted to at least capture large displacement response in one direction. Walls 2-4 had asymmetric strengthening in the wall corners as indicated in Fig. 1. Wall 5 had a symmetric layout as indicated in Fig. 6(e), but its performance differed in the two directions of loading. The asymmetric behaviour of Wall 3, as seen in Fig. 5(c), was partially caused by extensive sliding in the push direction. Note that (1) all lateral displacement data depicted in Fig. 5 were corrected for sliding displacement, thus representing only the wall flexural and shear deformation behaviour and (2) the corrected lateral displacement has been used as reference in all graphs and tables.

Damage pattern and failure mode

Gradual strength degradation was observed for all walls (except Wall 5), attributed to spalling of face shells and crushing of the grout core. Large displacement capacity was observed with reliable wall resistance for drifts, γ_u, ranging from 0.7% to more than 2.6%, refer to Table 2. A relatively more sudden strength degradation was observed for Wall 5 in the push direction when going beyond D12 (30 mm), caused by rapid strength degradation of the ordinary

masonry block (U200) just above the high strength block (lower right wall corner as shown in Fig. 6(e)). Crack patterns after failure, depicted schematically in Fig. 6, indicated that the extent of damage was confined to the lowest two masonry courses in the toe regions, with the majority of damage concentrated in the lowest course. Damage to the masonry units immediately above the lowest course generally was limited to vertical splitting cracking near the wall end. The inclined cracking observed in Wall 2 (no shear reinforcing), Wall 5 (no shear reinforcing) and Wall 3 (with shear reinforcing) suggests that shear reinforcement is necessary for walls of present dimensions, in order to avoid sporadic cracking.

Figs. 6(b) and 6(e) show inclined cracks that appeared while pulling Walls 2 and 5 to -D2 (-5 mm) and -D4 (-10 mm) respectively. It is believed that these cracks were caused by large localised splitting forces associated with the prestress anchorage at the centre of the loading beam. The cracks did not develop further during testing, possibly due to transverse restraint provided by the loading beam.

Sliding

Fig. 7 presents sliding displacement envelopes (recorded sliding at excursion peaks) for three of the wall tests; again it is noted that lateral displacement on the horizontal axis has been corrected for sliding displacement. Fig. 7 shows that significant sliding occurred for Walls 1 and 2 throughout the tests, and that sliding increased gradually with lateral displacement. Both tests were conducted in a monotonic fashion at large displacement levels, which naturally did tend to increase the total sliding displacement due to the absence of excursions in the opposite loading direction that could reverse the sliding that occurred. Sliding displacements were negligible for Wall 3 for all cyclic excursions, but once the wall had failed in the pull direction -D10 (-30 mm), the wall slid further and further in the push direction. This was partially due to reduced efficiency of the dowel bars as the compression zone integrity deteriorated. There was no indication of significant wall sliding relative to the

foundation for Wall 4 (not shown in Fig. 7), attesting to the efficiency of the dowel and energy dissipater bars to block sliding. Negligible sliding occurred for Wall 5 (not shown in Fig. 7) until after D16 (40 mm) where push testing was terminated, and was relatively small thereafter.

Gradual deterioration of the foundation beam roughness had occurred as the testing of Series 2 walls progressed (the foundation beam was also used testing of the Series 1 walls reported in Laursen and Ingham (2001)), thus reducing the shear friction along the wall/base construction joint.

Prestressing force

The prestressing tendon force histories (sum of force of all tendons) for all walls are plotted against the lateral displacement in Fig. 8. For reference, the nominal yield strength for one 23 mm VSL CT stress bar is approximately 385 kN.

Walls 1, 2 and 5 had the tendons rigidly anchored in the foundation and on top of the loading beam, and did exhibit tendon yielding during testing, as indicated in Figs. 8(a), 8(b) and 8(e). It is seen that the first significant total tendon force loss (more than 5% of the initial force) for these walls occurred after lateral wall displacements to about ±10 mm, in all cases roughly corresponding to first yield of the extreme tendons when considering the wall as a rigid body rocking about the wall corners. At the conclusion of testing of Walls 1, 2 and 5, between 20% and 50% of the initial total prestressing force remained.

Figs. 8(c) and 8(d) show the prestressing tendon force history for Walls 3 and 4. These figures reveal that the prestressing force at the excursion displacement peaks amounted to approximately 610 kN and 640 kN for Walls 3 and 4, respectively, or about 5% higher than the initial prestress force value.

Vertical masonry strain

During testing the vertical strain was recorded along the bottom of the walls using the instrumentation shown in Fig. 4.

For Walls 1 and 5 the instruments F1, F17, F21, F25 and F9 (level 1 instrumentation) spanned between the foundation beam and the middle of the first masonry course (100 mm gauge length). Likewise, instruments F2, F18, F22, F26 and F10 (level 2 instrumentation) spanned between the middle of the first and second courses. This implies that both level 1 and level 2 vertical strain measurements for these walls included a component of vertical deformation of the first course, the course where most inelastic action occurred. Strain measurements for all other walls were recorded between bed joints of one course for CP200 configurations and between bed joints of two courses for CP100, i.e. 200 mm gauge length.

Strain measurements revealed that vertical strain varied nearly linearly along the length of the walls for all displacement levels. It was found that this was not the case for Wall 5 for loading above $\pm V_f$, presumably because of the stiffness incompatibility between high strength and ordinary masonry units.

The general trend for CP200 and CP100 masonry for low-level response were recorded extreme fibre strain of approximately 0.003 for readings below D2 and approximately 0.004-0.006 for D2. The extreme fibre strain for large displacement response ranged from 0.01 to 0.08. Strains at level 2 remained below 0.0012 for Walls 2, 3 and 4, thus indicating elastically responding masonry. Measurements at level 2 for Walls 1 and 5 suggested strains higher than 0.0015, however, as noted above, these measurements were taken by instrumentation that also picked up deformation in the first masonry course.

Measurements of vertical strain above level 2 indicated elastic masonry response at these locations (vertical strain significantly lower than 0.001). This attests that the vertical extent of

the compression zone undergoing plastic deformation remained rather short, of the order of 200 mm to 400 mm.

Extreme fibre vertical strains in the flexural compression zones (the toe) of the walls were evaluated for the following wall states: (1) at nominal flexural strength, V_f, (2) at maximum strength, V_{max}, and (3) at ultimate displacement, d_u. The strains presented in Table 3 were measured in the lowest 100 to 200 mm of the walls. Results for Wall 5 are not included.

It is acknowledged that vertical strain readings at level 1 were influenced by base sliding to some degree and were associated with some degree of uncertainty for displacement levels above D2 where significant deterioration of the masonry units may have affected instrument reading.

DISCUSSION

Flexural response

Fig. 5 indicates that the developed flexural strength V_{max} (base shear corresponding to the maximum moment) exceeded the predicted flexural strength V_f in all wall tests. Comparing in Fig. 9 the force-displacement envelopes (peak response of first excursion cycle for each displacement level) for Walls 2, 3 and 5, which had similar dimensions and prestressing properties, it is seen that Walls 2 and 5 developed higher strength than Wall 3. This directly resulted from the tendon force in Wall 3 being kept constant during testing, prohibiting tendon force increase due to flexural action. The performance of Walls 2 and 3 differed in the push direction (positive displacement), despite both featuring CP100 masonry in the compression zone, with Wall 3 developing a larger maximum displacement as shown in Fig. 9. This was expected as a result of the lower axial load in Wall 3. It is difficult to compare the pull-direction response of Walls 2 and 3 because Wall 2 test results in that direction were significantly influenced by the testing regime, which consisted of monotonic pull-direction

testing following the completion of push-direction testing. It is of considerable interest that Wall 5 performed similar to Wall 2 in the push direction and possibly better than Wall 2 in the pull direction. The implication is that performance using a single high strength block in each wall corner is comparable to that obtained using confining plates. Embedding high strength blocks in the lower corners appears to be a less laborious solution compared with embedment of confining plates.

Comparing the response of Walls 3 and 4 in Fig. 9, it is clear that the latter developed the highest strength. This was due to the energy dissipaters built into Wall 4 that had a nominal yield strength of 2 x 100 kN = 200 kN. Adding this force to the applied prestressing force of approximately 600 kN suggests that the strength of Wall 4 would be approximately (600 kN + 200 kN)/600 kN = 1.33 times higher than that of Wall 3. Fig. 9 and Table 2 confirm this. The displacement capacity of Wall 4 was lower than that of Wall 3 in the push direction (CP100 masonry), a direct effect of the larger flexural compression force generated in Wall 4 due to the addition of energy dissipation bars. In the pull direction the displacement capacity of Wall 4 was superior to that of Wall 3. Comparison of the performance of CP200 vs. CP100 for these two tests favours CP100 in terms of displacement capacity.

Tendon yielding

Tendon yielding was expected for all walls without axial load control. Significant prestress loss occurred for these walls, as illustrated in Fig. 8. At the peaks of excursions, Walls 1 and 2 generally developed a total tendon force higher that the initial tendon force (Figs. 8(a) and 8(b)). Wall 5 exhibited some tendon force increase at peak response. However, as wall toe degradation initiated, the total tendon force at displacement peaks started to decline to levels below the initial total tendon force. Despite tendon force loss due to yielding, the walls continued to return to their initial alignment (disregarding sliding), as indicated in Fig. 5.

No tendon yielding occurred for Walls 3 and 4 as a result of active control of the tendon force. Modest tendon force variation was recorded as shown in Figs. 8(c) and 8(d) as a result of friction in the hydraulic system.

Vertical masonry strain

Table 3 shows the vertical strain recorded in the plate confined walls at different stages of the tests. It is seen that the calculated masonry strains corresponding to the nominal flexural condition, V_f, ranged from 0.0019 to 0.0055 for CP200 and from 0.0016 to 0.0027 for CP100. These results do not conform with the code-defined nominal flexural strength condition set out by NZS 4230:1990 for confined masonry, that specifies a useable extreme fibre masonry strain at nominal flexural strength of 0.008.

The masonry strain recorded at V_{max} ranged from 0.0052 to 0.0190 for CP200 and from 0.0037 to 0.023 for CP100. Thus there was a large variation in vertical strain at this limit state. It is the opinion of the authors that at this limit state the masonry fibres at the extreme ends of the walls still provided some axial strength, resisting the overturning moment.

Table 3 indicates that masonry extreme fibre strains ranged from 0.024 to 0.070 for CP200 and from 0.033 to 0.068 for CP100 at the ultimate displacement, d_u. These values are of course of theoretical character as the toe regions were damaged at this stage, so that those strains should not be regarded as the reliable ultimate strain capacity of concrete masonry. The results do nevertheless suggest that masonry strains far beyond those related to nominal flexural strength can be expected for rocking wall systems, while still providing significant axial strength. At this limit state the effective flexural neutral axis at the wall base had migrated towards the middle of the wall.

Hysteretic energy dissipation

Comparison of Figs. 5(c) and 5(d) illustrates the effect of the energy dissipation bars in Wall 4. The area enclosed by the force-displacement loading and unloading curves for each excursion for Wall 4 was increased considerably by yielding of the energy dissipation bars, as significant yielding commenced going to displacement level 4 (17 mm). The energy dissipated in each excursion (half cycle) due to hysteresis can be quantified by integration of the area enclosed by the loading and unloading curves. Results of such integration applied on Walls 3 and 4 are illustrated in Fig. 10. The figure shows the cumulated energy dissipation as a function of the wall lateral displacement history. Fig. 10(a) illustrates that the energy applied to displace Wall 3 from zero displacement (original alignment) to the peak of an excursion, was mostly recovered upon subsequent unloading. On the contrary, Wall 4 response shown in Fig. 10(b) suggests that only about 30-50% of the energy exerted by the loading system displacing the wall from zero displacement to a displacement peak was recovered upon subsequent unloading. As a numerical example, the total energy dissipated in the last two cycles shown in Figs. 10(a) and 10(b) has been calculated. The circular and square markers illustrate the beginning and end of the two displacement cycles to ±30-35 mm, respectively. Calculation shows that Wall 3 dissipated 4.8 kJ while Wall 4 dissipated 15.5 kJ. Clearly the hysteretic energy dissipation was increased substantially by the inclusion of the energy dissipation bars. Little sliding was measured for the walls depicted in Fig. 10 in the displacement range shown, thus this was not a source of 'parasitic' energy dissipation.

Sliding propensity

Wall sliding was measured for all walls, except Wall 4. Elimination of this phenomenon was sought by the addition of sliding blocking plates placed adjacent to each end of the walls and by embedment of dowel bars. Results from testing of Walls 1 and 2 with sliding blocking plates mounted on the foundation showed that solution to be inadequate. Once distress of the

compression zone had initiated, the compression zone could resist little lateral force as the wall slid towards the sliding blocking plates. Sliding for Wall 5 did not initiate before integrity of the high strength blocks was lost. This occurred after approximately 40 mm of displacement. Again, the sliding blocking devices did not offer much restraint.

Walls 3 and 4 had dowel bars embedded in both compression zones of the wall as shown in Fig. 1. These bars offered sufficient sliding restraint for Wall 3 in the pull direction (CP200), however when the CP200 end had failed and monotonic testing in the push direction was instated for the remainder of the test, sliding initiated gradually as the CP100 compression zone integrity gradually degraded. It appears that the dowel bars worked satisfactorily in the push direction until a displacement of about 45 mm (1.6% drift) was reached.

It is concluded that adequate shear friction between wall and foundation requires intentional roughening of the wall to foundation interface. Unbonded dowel bars, possibly in conjunction with longer continuous bars (in this case energy dissipation bars), appeared a viable option for adding further sliding resistance to the shear friction provided by the masonry/concrete foundation interface.

Initial stiffness

Estimation of initial stiffness is of considerable importance for serviceability and seismic loading. Fig. 11 shows curves for Walls 2-5 presented in this article and for two walls from the previous testing series discussed in Laursen and Ingham (2001), notably FG:L3.0-W15-P2C (referred to hereafter as P2C) and FG:L3.0-W15-P2E (referred to hereafter as P2E). The curves relate to the wall secant stiffness at the theoretical first cracking limit state (decompression of extreme tension end of wall). It is seen in the figure that the initial stiffness varies little between the walls. This is not surprising because the wall initial stiffness theoretically only depends on the wall dimensions and the masonry elastic properties, and

these were nearly identical for all tests. The average initial stiffness (flexural + shear deformation) for the walls shown in Fig. 11 was 238 kN/mm compared, to a theoretical elastic stiffness of 354 kN/mm (using elastic modulus of E_m = 15 GPa, Poisson's ratio of ν = 0.2 and P+N = 641 kN). The average measured wall initial stiffness was 33% lower than the theoretical one.

Comparison with unconfined PCM wall tests

Walls P2C and P2E from Series 1 (reported in Laursen and Ingham, 2001) had two prestressing bars embedded, the P2C bars being concentrically located identical to all wall tests presented herein (±400 mm) and the P2E bars being eccentrically located at ±1200 mm, and with both walls featuring unconfined ordinary masonry units throughout (U200). P2C results facilitate direct comparison with Walls 2 and 5 because of similar dimension and prestressing layout. Fig. 12 shows the force-displacement envelopes for these walls.

Examining wall response in the push direction (positive displacement), the following observations are made: all walls developed similar strength; strength degradation for P2C and P2E initiated at approximately 0.4% drift while strength degradation for the series 2 walls initiated at about 0.9% drift; the ultimate displacement capacity (at strength degradation to $0.8V_{max}$ shown as dashed lines) for Walls 2, 5 and P2E were similar at approximately 1.2% drift; P2C had a displacement capacity of about 0.8% drift. It is therefore concluded that CP100 (half height confining plates) and HB (high strength block) solutions performed significantly better than U200 for both P2C and P2E in terms of initiation of strength degradation, and CP100 and HB performed better in terms of ultimate displacement capacity in comparison with U200 for P2C.

Examining wall response in the pull direction (negative displacement), similar observations are made: all walls developed similar strength (except for Wall 2 that was influenced

significantly by base sliding, rendering the results difficult to compare with those from the other wall tests); rapid strength degradation for P2E initiated at approximately 0.3% drift while strength degradation of Wall 5 and P2C was rather gradual; the ultimate displacement capacities (at strength degradation to $0.8V_{max}$ shown as dashed lines) for Wall 5, P2C and P2E were approximately 1.4%, 1.1%, and 0.5% drift, respectively. It is therefore concluded that the HB solution performed significantly better than U200 for both P2C and P2E in terms of initiation of strength degradation and ultimate displacement capacity. It cannot be directly concluded from Fig. 12 that CP200 performed better than U200, however, the large displacement capacity in the pull direction for Wall 2 also suggest that CP200 masonry outperforms U200 masonry by a significant margin.

RECOMMENDATIONS

Further research is required to develop a suitable expression for the magnitude of tendon force increase to be adopted in ultimate flexural strength calculations for walls with unbonded tendons. Also, dynamic shake table testing of post-tensioned walls would greatly facilitate the development of analytical techniques to model the seismic response of this wall type. In particular, appropriate levels of damping need to be established in order to better determine during design whether supplementary damping is required to limit ultimate drifts.

Practical design solutions and details need to be articulated to structural designers for both residential concrete masonry construction, and for commercial and industrial applications.

CONCLUSIONS

It is concluded that strengthening of the flexural compression zones of fully grouted unbonded post-tensioned concrete masonry walls successfully improved the wall displacement capacity and delayed the onset of strength degradation in comparison with PCM walls of similar dimensions made with unconfined masonry. The maximum wall strength remained

insensitive to strengthening of the compression zone as strength was influenced by the level of prestress and provision of vertical reinforcement, and not by the flexural compression strength.

The walls exhibited a nearly non-linear elastic behaviour dominated by rocking response. The exception was Wall 4 that exhibited rocking response with non-linear elasto-plastic behaviour due to the presence of energy dissipation devices.

Large drift capacities were measured, 0.7% to 2% for directions with CP200 corners engaged, 1.1% to 2.6% with CP100 corners engaged and 1.1% to 1.4% with high strength block corners engaged. This clearly attests to consistent improvement of wall displacement capacity using confining plates or high strength corner units. The highest performing solution was CP100.

Only localised damage occurred, making earthquake damage easy to repair. Nearly all damage occurred to the lowest masonry course for CP200 and CP100. This is supported by the vertical strain measurements that suggested little inelastic masonry response above the lowest 200 mm of the walls. The high strength masonry units appear to have shifted masonry crushing to the second masonry course above the foundation (U200) because of their very high strength.

One wall had ‘dog-bone’ energy dissipation devices embedded. This simple device proved successful and worked as expected. A threefold increase of hysteretic damping was achieved at large displacement levels. The inherent simplicity and insensitivity to construction tolerance of the ‘dog-bone’ type device makes it a desirable construction option.

Tendon force loss due to yielding may occur at relatively low wall drift ratios for squat walls. Even after tendon yielding, reliable and self-centring wall behaviour is expected.

Measurements at nominal flexural strength suggest extreme masonry fibre strain in the order of 0.0035 for CP200 and 0.0020 for CP100. Both values are substantially lower than 0.008 as stipulated by NZS 4230:1990 for confined masonry. At ultimate displacement, strains as high as 0.046-0.050 were measured for both CP200 and CP100. At this stage the extreme masonry fibres no longer carried axial load as face shell spalling had occurred.

It was concluded that adequate shear friction between wall and foundation requires intentional roughening of the wall to foundation interface. Dowel bars are effective for adding further sliding resistance.

Shear reinforcing should be embedded in PCM walls to reassure integrity of the masonry panel, though not necessarily needed for strength.

ACKNOWLEDGEMENTS

This research was funded by direct industry sponsors W. Stevenson and Sons Ltd., Firth Industries Ltd., Ready Mix Concrete Ltd. and VSL (Aust) Pty. Ltd., by the industry organisations NZCMA and CCANZ, and by the University of Auckland. Their contributions are gratefully acknowledged.

DISCLAIMER

The opinions and conclusions presented herein are those of the authors, and do not necessarily reflect those of the University of Auckland or any of the sponsoring parties to this project.

REFERENCES

Laursen, P.T. (2002), *Seismic Analysis and Design of Post-tensioned Concrete Masonry Walls*, PhD dissertation, March, Department of Civil and Environmental Engineering, University of Auckland, New Zealand.

Nakaki, S.D., Stanton, J.F. and Shritheran, S. (1999), *An overview of the PRESSS Five-Story Precast Test Buildin*g, PCI Journal, March-April, 26-39.

Holden, T., Restrepo, J., and Mander, J.B. (2003). "Seismic performance of precast reinforced and prestressed concrete walls." *J. Struct. Engrg.*, ASCE, 129(3), 286-296.

Kurama, Y.C., Sause, R., Pessiki, S., and Lu, L.-W. (2002) "Seismic response evaluation of unbonded post-tensioned precast walls." *ACI Struct. J.*, 99(5), 641-651.

Laursen, P.T. and Ingham, J.M. (2001), *Structural Testing of Single-Storey Post-Tensioned Concrete Masonry Walls*, The Professional Journal of The Masonry Society, Vol. 19, No. 1, September, The Masonry Society, Boulder, Colorado, 69-82.

Laursen, P.T., Davidson, B.J. and Ingham, J.M. (2002), *Seismic analysis of prestressed concrete masonry shear walls*, Proceedings of the 12th European Earthquake Conference, September, London, England.

Priestley, M.J.N. and Elder, D.M. (1983), *Stress-strain curves for Unconfined and Confined Concrete Masonry*, ACI Journal, Vol. 80, No. 3, May-June, 192-201.

Park, R. (1989), *Evaluation of Ductility of Structures and Structural Assemblages for Laboratory Testing*, Bulletin of NZNSEE, Vol. 22, No. 3, Sept, 155-166.

NZS 4230:1990, *Code of Practice for the Design of Masonry Structures*, Standards Association of New Zealand, Wellington.

Paulay, T., and Priestley, M.J.N. (1992), *Seismic Design of Reinforced Concrete and Masonry Buildings*, John Wiley & Sons Inc.

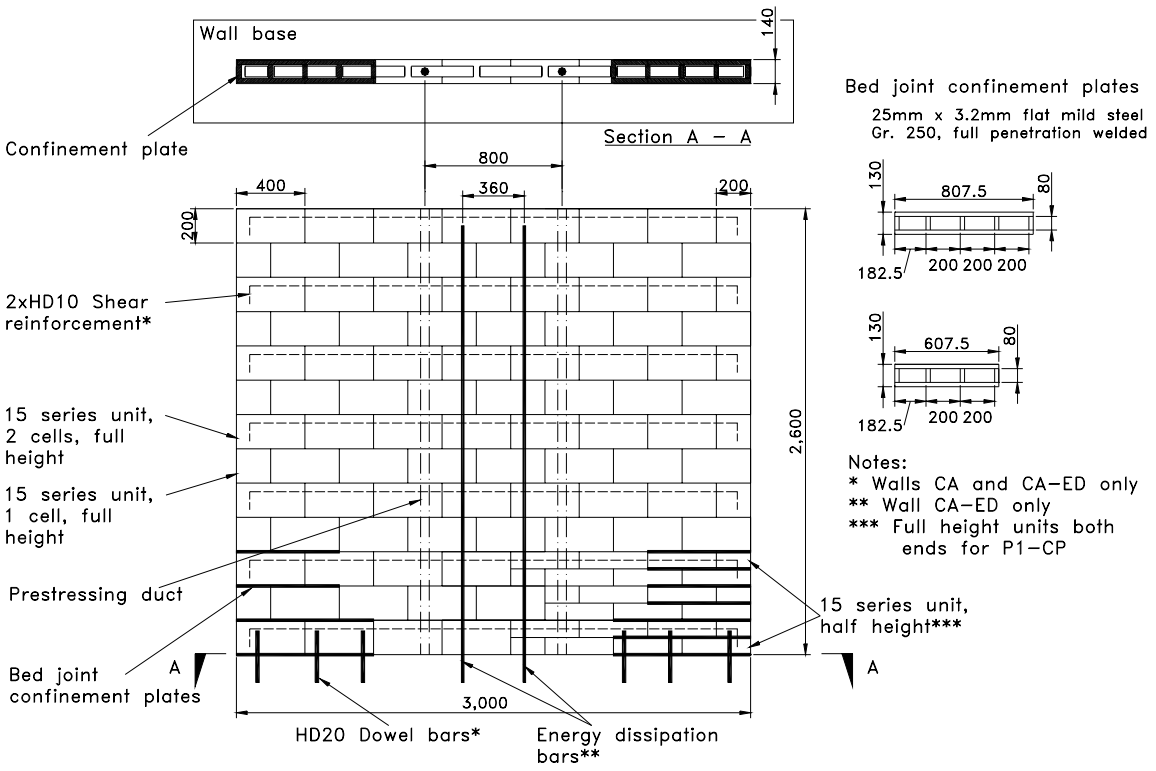

Fig. 1-Geometry of walls having confinement plates.

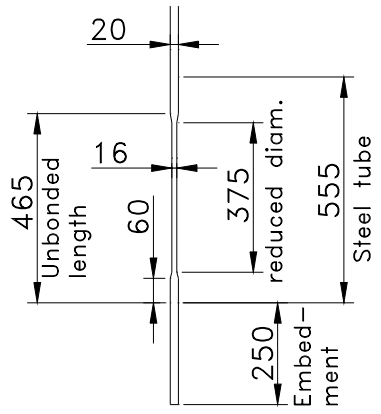

Fig. 2-Wall 4 energy dissipation bars

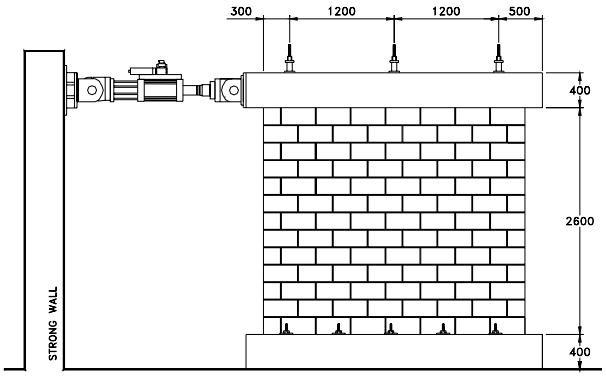

Fig. 3-Test setup

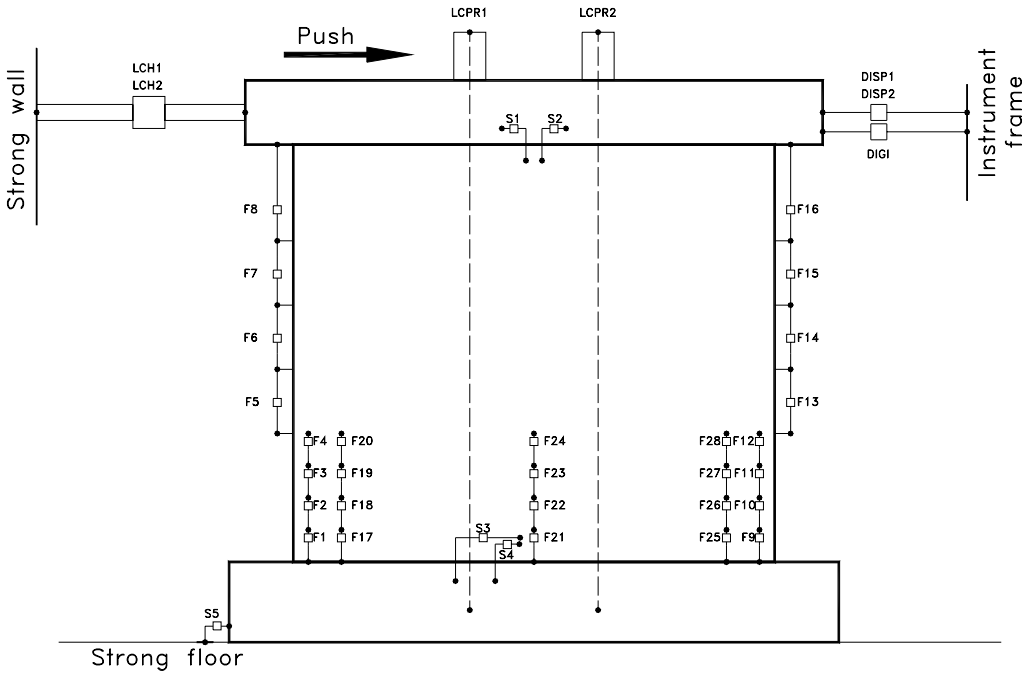

Fig. 4-Typical Instrumentation

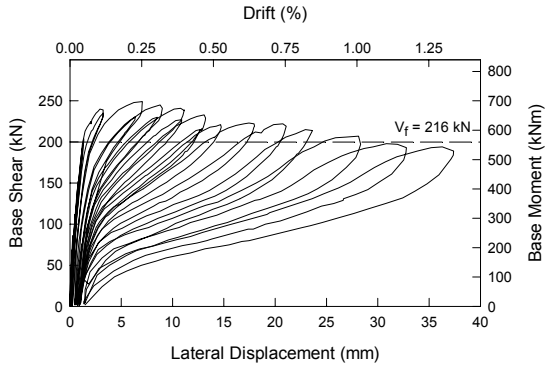

(a) Wall 1. FG:L3.0-W15-P1-CP

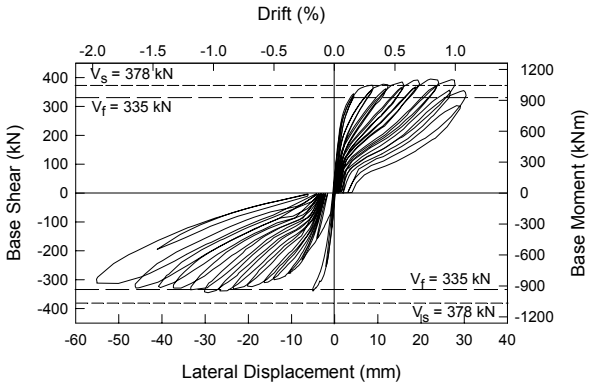

(b) Wall 2. FG:L3.0-W15-P2-CP

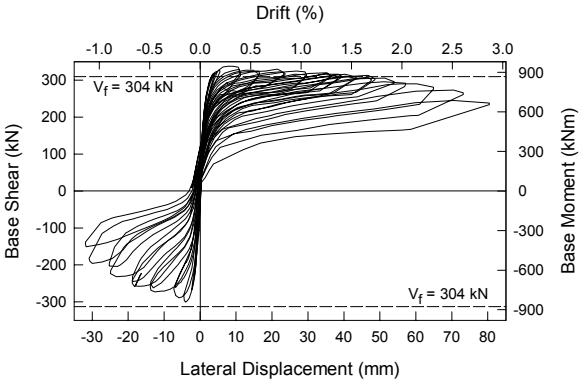

(c) Wall 3. FG:L3.0-W15-P2-CP-CA

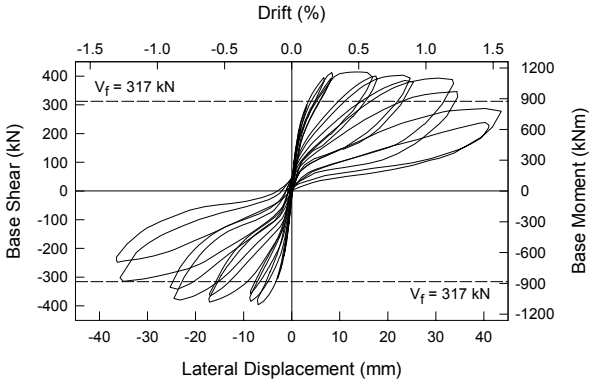

(d) Wall 4. FG:L3.0-W15-P2-CP-CA-ED

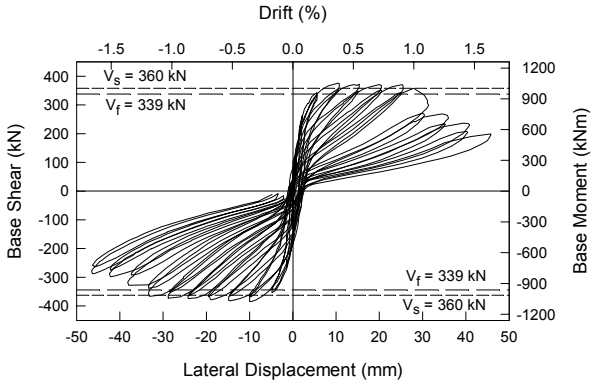

(e) Wall 5. FG:L3.0-W15-P2-HB

Fig. 5-Force-displacement histories

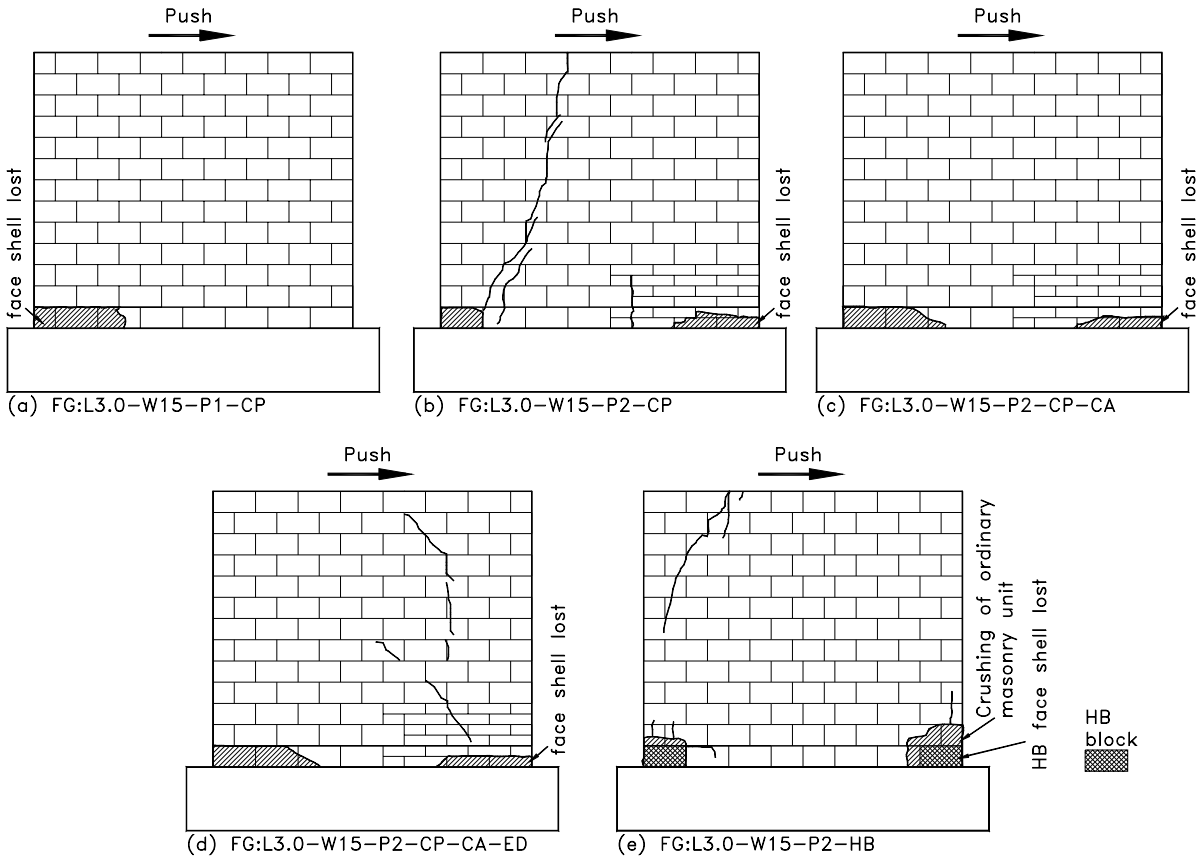

Fig. 6-Damage accumulation at failure

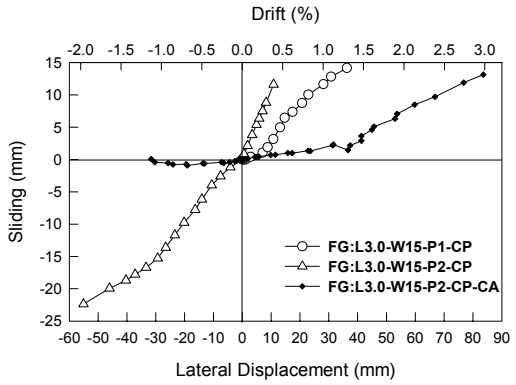

Fig. 7-Relative sliding between wall and base, envelopes

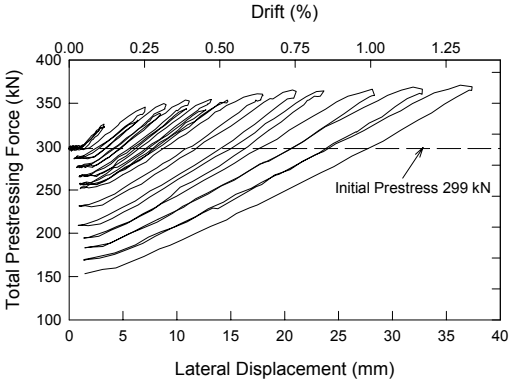

(a) Wall 1. FG:L3.0-W15-P1-CP

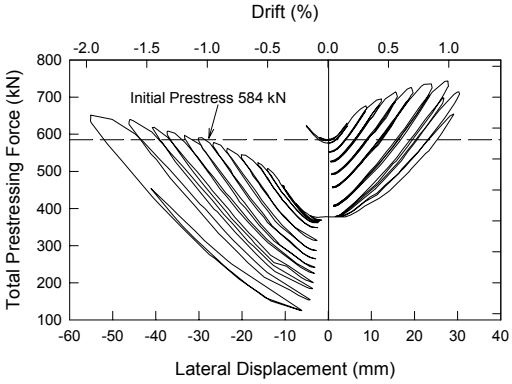

(b) Wall 2. FG:L3.0-W15-P2-CP

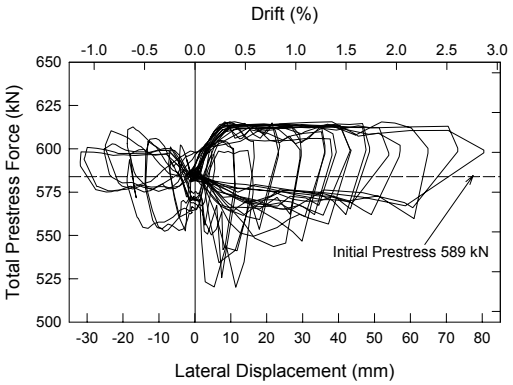

(c) Wall 3. FG:L3.0-W15-P2-CP-CA

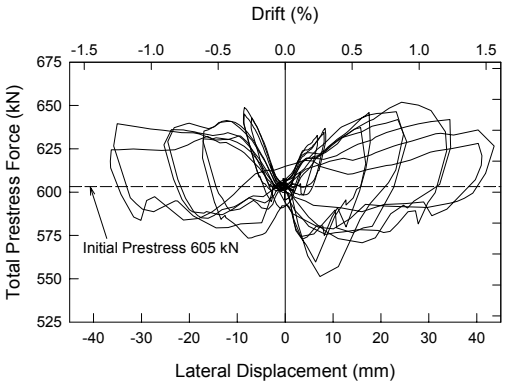

(d) Wall 4. FG:L3.0-W15-P2-CP-CA-ED

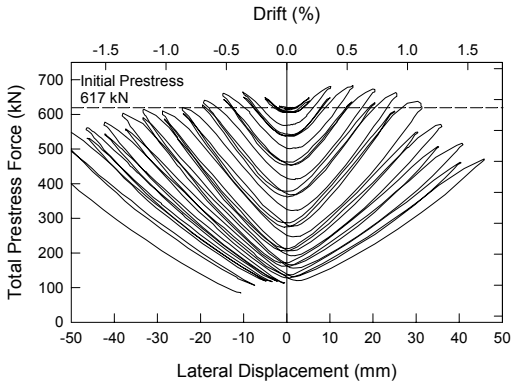

(e) Wall 5. FG:L3.0-W15-P2-HB

Fig. 8-Prestressing force histories

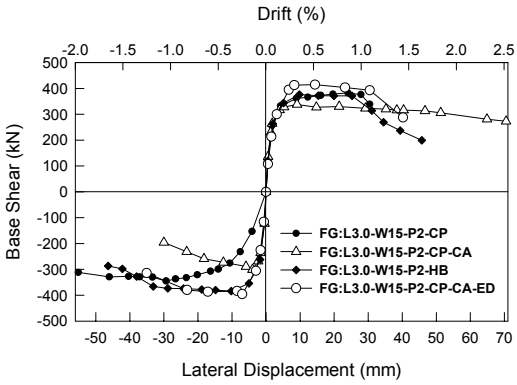

Fig. 9-F-D envelopes for Walls 1-4

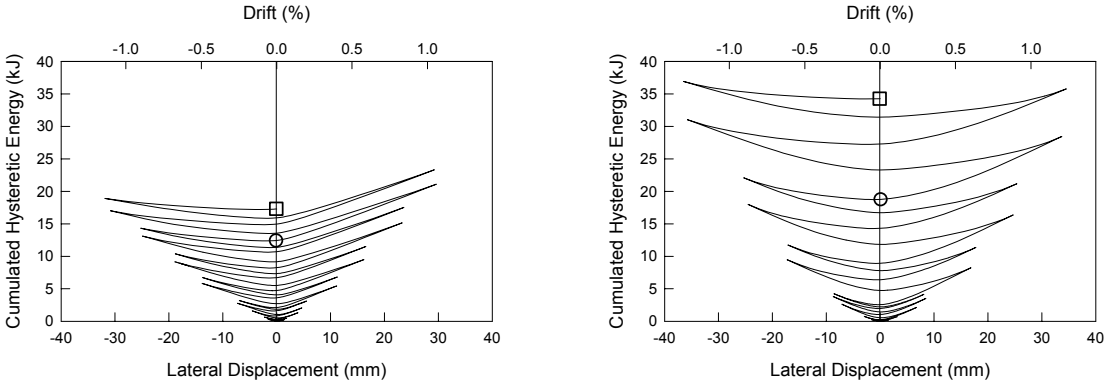

(a) Wall 3. FG:L3.0-W15-P2-CP-CA (b) Wall 4. FG:L3.0-W15-P2-CP-CA-ED

Fig. 10-Cumulated hysteretic energy dissipation

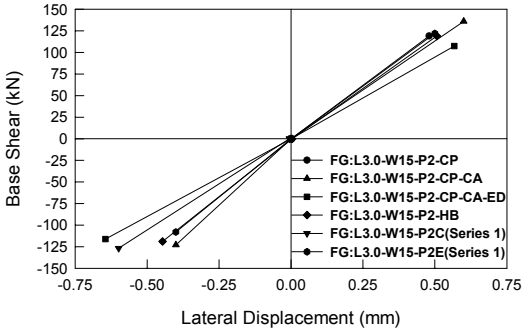

Fig. 11-Initial wall stiffness

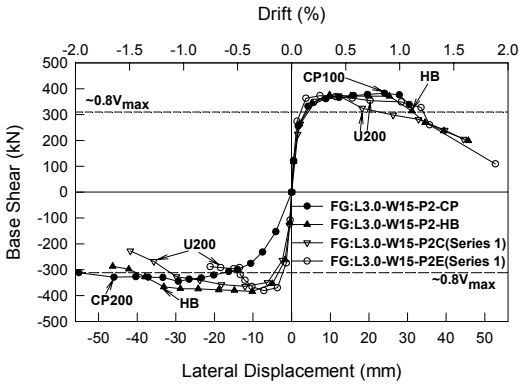

Fig. 12-Comparison of F-D envelopes for Series 1 and Series 2 walls

TABLE 1-Wall specifications

Wall	f'_m, masonry strength			Age at DOT	No. of tend.	initial steel stress f_{ps}	initial tendon force P	axial force ratio[#] f_m/f'_m
	U200	CP200	CP100					
1. FG:L3.0-W15-P1-CP	18.2	21.7		13	1	720	299	0.044
2. FG:L3.0-W15-P2-CP	15.9			63	2	703	584	0.094
3. FG:L3.0-W15-P2-CP-CA	19.1	19.8	18.6	38	2	708	588	0.078
4. FG:L3.0-W15-P2-CP-CA-ED	19.3	19.9		31	2	727	604	0.080
5. FG:L3.0-W15-P2-HB	12.5			32	2	743	617	0.125
	MPa	MPa	MPa	days	-	MPa	kN	-

[#]based on U200 and $f_m = (P+N)/(l_w b_w)$

TABLE 2-Predictions and Results

Wall	Prediction		Results						Comments
	V_f	V_s	Dir./Conf.	D1	V_{max}	d_{vmax}	d_u	γ_u	
1. FG:L3.0-W15-P1-CP	216	325	Pull/CP200	1.7	-249	-7.1	-32.7	0.012	Masonry crushing, flexural failure, pull test only
2. FG:L3.0-W15-P2-CP	335	378	Push/CP100	2.5	395	22.2	30.4	0.011	Masonry crushing, diagonal crack, flexural failure
			Pull/CP200		-345	-29.3	-55.1	0.020	
3. FG:L3.0-W15-P2-CP-CA	309	806	Push/CP100	3.0	338	9.1	73.1	0.026	Masonry crushing, flexural failure
			Pull/CP200		-301	-4.0	-18.8	0.007	
4. FG:L3.0-W15-P2-CP-CA-ED	317	811	Push/CP100	4.3	414	14.4	34.5	0.012	Masonry crushing, flexural failure
			Pull/CP200		-396	-7.0	-35.0	0.013	
5. FG:L3.0-W15-P2-HB	339	360	Push/HB	2.5	376	10.5	31.4	0.011	Masonry crushing, diagonal crack, flexural failure
			Pull/HB		-384	-10.1	-38.1	0.014	
	kN	kN		mm	kN	mm	mm	-	

Note: sliding displacement subtracted from d_{vmax} and d_u

TABLE 3-Measured masonry vertical strain

Wall	Dir./Conf.	V_f		V_{max}	d_u
		displ.	strain	strain	strain
1. FG:L3.0-W15-P1-CP	Pull/CP200	-1.7	0.0035	0.0107	0.070*
2. FG:L3.0-W15-P2-CP	Push/CP100	1.7	0.0016	0.0230	0.036
	Pull/CP200	-2.0	0.0019	0.0190	0.055
3. FG:L3.0-W15-P2-CP-CA	Push/CP100	4.0	0.0016	0.0037	0.068
	Pull/CP200	-4.0	0.0029	0.0052	0.024
4. FG:L3.0-W15-P2-CP-CA-ED	Push/CP100	6.7	0.0027	0.0053	0.033
	Pull/CP200	7.0	0.0055	0.0116	0.050
		mm	-	-	-

Note: *extrapolation based on instruments F16 and F20